ACS OMEGA

Open Access

http://pubs.acs.org/journal/acsodf

Article

Wide-Range Synaptic Current Responses with a Liquid Ga Electrode via a Surface Redox Reaction in a NaOH Solution at Different Molar Concentrations

Dahee Seo,[‖] Seongyeon Kang,[‖] Heejoong Ryou, Myunghun Shin, and Wan Sik Hwang*

Cite This: *ACS Omega* 2023, 8, 41495−41501

Read Online

ACCESS | Metrics & More | Article Recommendations | Supporting Information

ABSTRACT: A liquid Ga-based synaptic device with two-terminal electrodes is demonstrated in NaOH solutions at 50 °C. The proposed electrochemical redox device using the liquid Ga electrode in the NaOH solution can emulate various biological synapses that require different decay constants. The device exhibits a wide range of current decay times from 60 to 320 ms at different NaOH mole concentrations from 0.2 to 1.6 M. This research marks a step forward in the development of flexible and biocompatible neuromorphic devices that can be utilized for a range of applications where different synaptic strengths are required lasting from a few milliseconds to seconds.

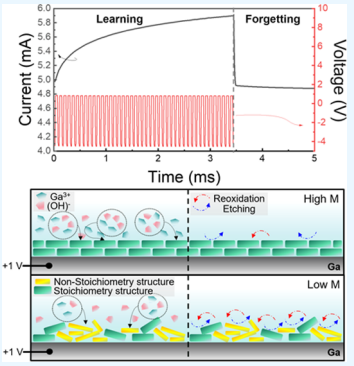

1. INTRODUCTION

The von Neumann architecture has served as the basis of modern digital electronics for the last few decades.[1] It mainly consists of a central processing unit (CPU) and a memory unit. The CPU accesses the memory through a shared bus, which facilitates the transfer of data between the CPU and memory in both directions. This data transfer through the bus suffers from large latency and high power consumption, causing interconnect bottlenecks when working with large data sets.[2,3] With the advent of artificial intelligence (AI) that can perform cognitive tasks and offer predictions for the future, the von Neumann bottlenecks limit the performance of advanced electronics requiring real-time processing and computing such as big data analytics and machine learning.[4] To address the challenges of latency and power consumption inherent in the von Neumann architecture, new computational methodologies based on in-memory processing units (IMPUs) or processing in memory (PIM) have been proposed.[5] In the IMPUs or PIM architecture, the processing elements are integrated directly into the memory units, allowing computation to be performed on the data stored in the memory without data transfer between the CPU and memory through the bus. In short, this computing architecture allows CPU and memory functionality to occur within the same unit without the interconnect. Compared to the traditional von Neumann architecture, the IMPU/PIM architecture can considerably minimize latency and power consumption since there is no requirement to transfer data repeatedly between the CPU and memory.[6] This computational methodology replicates brain functions, and the resulting devices are accordingly referred to as neuromorphic computing and synaptic devices because of the functional similarity with neural synapses.[7] Synaptic devices are a key component of neuromorphic computing systems and can serve to achieve ultrafast and energy-efficient computing in neuromorphic systems. These synaptic devices use analog circuits to model the variable strength of synaptic connections in the brain, enabling them to perform functions such as learning, memory, and pattern recognition. Unlike traditional memory devices that use binary information, those reported synaptic devices are not just binary on or off processes. In the biological system, information is transferred from one neuron to another through synapses. The strength of each synapse is represented by its synaptic weight that is represented as analog values and is used to control the amount of influence that one neuron has on another. The synaptic weight plays a crucial role in neuromorphic devices, which enable the system to process information in a way that is more like natural processing. So far, various synaptic devices have been reported with its own advantages and challenges, including resistive switching memory,[8−12] phase-changing memory,[13−15] ferroelectric memory,[16−19] electrochemical memory,[20−25] and charge trap memory.[26−28] Resistive switching memory implemented

Received: July 24, 2023
Revised: October 5, 2023
Accepted: October 11, 2023
Published: October 23, 2023

synaptic weights in neuromorphic systems, where the strength of a synapse is proportional to the resistance of the memory element.[8−12] Phase-change memory implemented synaptic weights by varying the crystalline state of the material to adjust the strength of the synapse, which can switch between amorphous and crystalline states to store data.[13−15] Ferroelectric memory can vary the polarization state of the material to adjust the strength of the synapse, which can switch between two stable polarization states to store data.[16−19] Electrochemical memory implemented synaptic weights by controlling the flow of ions across the junction,[20−25] where the strength of a synapse can be adjusted by changing the concentration of ions at the synaptic junction. These devices are electronic devices that use ions rather than electrons to conduct electricity. Charge trap memory varied synaptic weights by controlling the number of trapped charge carriers to adjust the strength of the synapse.[26−28] These reported synaptic devices have shown promise in terms of energy efficiency, scalability, and compatibility with the current technology.

Very recently, an ionic device using liquid Ga was made to resemble neural spike signals, which is beneficial for organ cell−machine interface systems because Ga is biocompatible and flexible at room temperature.[29,30] Depending on the specific application, synaptic functions with different decay constants are required for synaptic devices because synaptic functions with different decay constants can affect the temporal dynamics of the network and its ability to perform certain computations, such as short-term memory or pattern recognition.[31] Synaptic decay refers to the gradual decrease in the strength of a synaptic connection over time. For example, different decay constants can help the network distinguish between phonemes that have similar temporal patterns but different durations. In fact, the human brain utilizes a wide range of synaptic current decay from 1 ms to 1 s.[32] Different types of synaptic currents serve different functions in the brain. Fast decay time involves the rapid transmission of information between neurons, which can be used to filter out noise and unwanted signals. On the other hand, slow decay times are involved in more complex neural processes such as learning and memory. In previous studies, different decay characteristics have been demonstrated using different materials,[33] crystallinity,[34] defects,[35,36] and bias voltages.[29] In this study, we demonstrate a liquid Ga-based synaptic device using two-terminal electrodes in different NaOH solutions that can generate different synaptic current responses. The proposed devices exhibited a wide range of current decay times from 60 to 320 ms in different NaOH moles.

2. MATERIALS AND METHODS

The detailed experimental conditions were described in a previous study.[29] A drop (100 μL) of liquid Ga (99.999% from Sigma-Aldrich) and a Cu plate was used as a metal electrode. The liquid Ga formed a small spherical bead with a diameter of ∼1 cm. The two electrodes, separated by 3 mm with a canal width of 1 mm, were submerged in a NaOH solution (Daejung Chemicals & Metals Co.) at different molar concentrations (0.2, 0.4, 0.8, 1.0, 1.3, and 1.6 M). The Cu electrode was grounded while a voltage was applied to the Ga electrode. The Ga liquid metal moved toward the cathode when the applied voltage was higher than 1 V. This movement could be explained by several factors such as differences in the electrochemical potential or surface tension of the metal and the solution.[29] When the voltage was in the range from −2 to 1 V, the Ga ions in the solution were oxidized at the surface of the Ga electrode, forming a thin layer of solid Ga-based oxide on the Ga surface. Subsequently, the formed Ga oxide tends to be dissolved again in the solution due to the inherent nature of NaOH.[29] The Ga-based oxide was found to be etchable in both acidic and basic environments. The oxide dissolves in the acid solution through a reaction with H^+ ions, resulting in the production of soluble Ga^{3+} ions and water. Similarly, in basic solutions, the oxide dissolves by reaction with OH^- ions, forming soluble gallate ions (such as $NaGaO_2$) and water. When the voltage was in the range from −2 to −5 V, the formed Ga-based oxide was electrically removed in the NaOH solution. When the voltage was less than −5 V, no significant change was noticed except for the gas bubbles that were generated due to the electrocatalytic water splitting. Electrocatalytic water splitting is a process that uses an electric current to split water molecules into hydrogen and oxygen gases. The NaOH container was made of polylactic acid using a three-dimensional (3D) printer (Flashfore Advantage 3). The pH values of 0.2, 0.4, 0.8, 1.0, 1.3, and 1.6 M were 12.01, 12.25, 12.45, 12.54, 12.59, and 12.65, respectively. It should be noted that NaOH is considered stable in normal conditions of use, but it is incompatible with metals such as Al, Sn, and Zn, as well as their alloys.[37] Oxygen in the air was able to diffuse into the NaOH solution and interact with the NaOH aqueous solution. The NaOH container with the Ga and Cu electrodes was heated to a hot chuck at 50 °C. All electrical measurements were conducted using a parameter analyzer (Keithley 4200-SCS).

3. RESULTS AND DISCUSSION

When a NaOH-based ionic channel was established between the Ga and Cu electrodes, as shown in Figure 1a, spontaneous

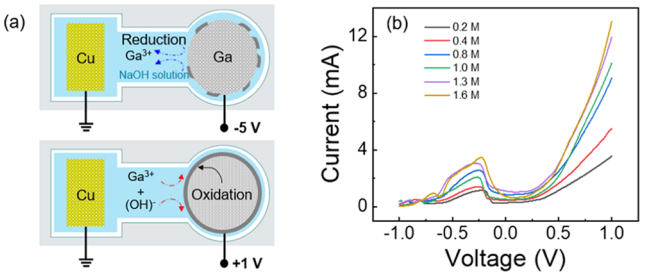

Figure 1. (a) Grounded Cu electrode with the voltage applied to the Ga electrode. These two electrodes, separated by 3 mm with a canal width of 1 mm, were submerged in a NaOH solution at different molar concentrations. The dimensions were determined because it could be achieved by the 3D printer. The NaOH container with Ga and Cu electrodes was heated to a hot chuck at 50 °C. (b) Current−voltage curve of a Ga electrode at different NaOH molar concentrations.

half-cell reactions took place on both sides, resembling those observed in a galvanic cell. As a result, the Ga electrode underwent oxidation and released electrons that were assumed to have been consumed by the Cu electrode via oxygen reduction. Following the oxidation of the Ga electrode, Ga-based oxide was subsequently formed on the Ga electrode.[38] It is known that a Ga-based oxide layer can also be dissolved in a NaOH solution. Under steady-state conditions, the reaction between the formation and dissolution of Ga-based oxide on

https://doi.org/10.1021/acsomega.3c05352
ACS Omega 2023, 8, 41495−41501

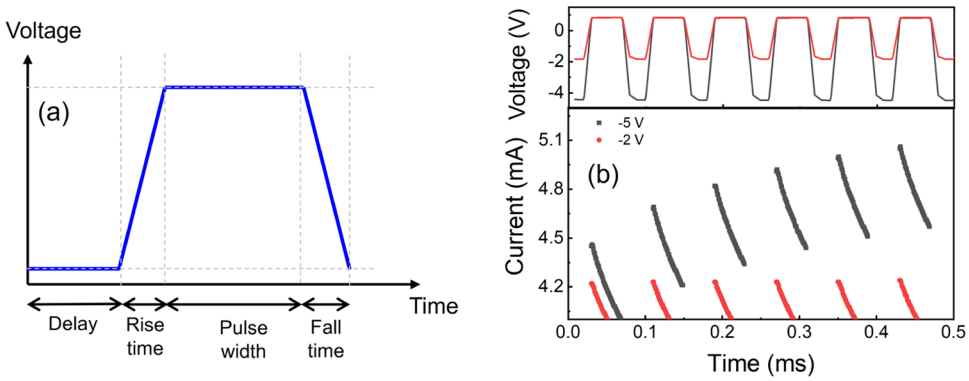

Figure 2. (a) Definition of the pulse-shaped stimulus. It is defined in terms of the rise and fall time, delay, and pulse width. (b) Synaptic behaviors of the Ga electrode in 1 M NaOH concentrations at a pulse width of 0.04 ms, a rise and fall time of 0.01 ms, and a delay time of 0.002 ms.

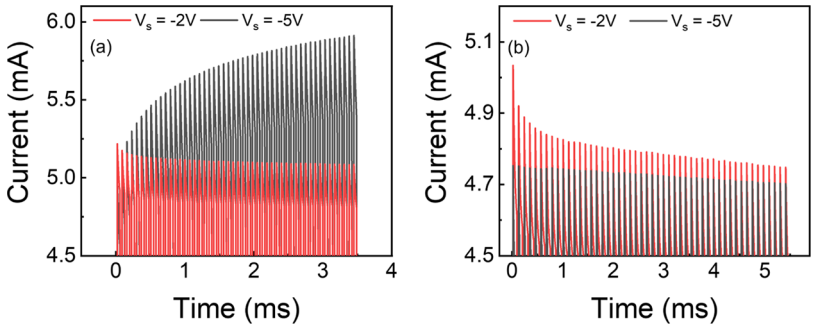

Figure 3. Generation of synaptic spike responses with a rise and fall time of 0.01 ms and a delay time of 0.002 ms at a pulse width of (a) 0.04 and (b) 0.08 ms.

the Ga surface eventually produces an extremely thin layer of Ga-based oxide. It is worth noting that when a voltage was applied to the Cu electrodes, similar oxidation and reduction peaks were observed as well,[39] indicating that Cu could also be dissolved in the NaOH solution. The Cu electrode was grounded while a voltage was applied to the Ga electrode. The Ga liquid metal moved toward the cathode when the applied voltage was higher than 1 V. This movement could be explained by several factors such as differences in the electrochemical potential or surface tension of the metal and the solution. In our previous work,[29] we demonstrated that this Ga-based oxide layer could be removed electrically by applying −2 to −5 V to the Ga electrode in the NaOH solution, which is called an electrochemical reduction. In the present study, when a negative voltage was applied to the Ga electrode, positively charged ions from the NaOH solution were attracted to the Ga-oxide surface. These electrically attracted ions reacted with the Ga-oxide layer, causing it to break down and dissolve in the NaOH solution. Conversely, when a positive voltage was applied to the Ga electrode, a Ga-based oxide was formed, leading to an anodic current peak (oxidation currents). Figure 1b shows the current−voltage curve of the Ga electrode in a NaOH solution at different molar concentrations. The voltage was adjusted from −1 to 1 V at a speed of 0.1 V/s. The results showed a small current hump at around −0.25 V regardless of molar concentration. This hump current represented anodic peaks and was attributed to the formation of a Ga-based oxide layer on the Ga surface. As the NaOH molar concentration increased, the peak current tended to increase, indicating that more oxidation occurred with the higher molar concentrations.

After analysis of the electrochemical oxidation current, as shown in Figure 1b, artificial synaptic behavior was demonstrated, imitating the behavior of a biological synapse. This is shown in Figure 2, which depicts the plasticity characteristics of the Ga electrode in the 1 M NaOH solution under different pulse conditions. Figure 2a presents a definition of a pulse-shaped stimulus including the rise and fall time, delay, and pulse width. When the voltage was changed from −2 to 1 V as shown in Figure 2b, the current level remained relatively constant. However, when the voltage was adjusted from −5 to 1 V in Figure 2b, the current value changed with an external stimulus exceeding the threshold value.

The results in Figure 2b indicated that the Ga electrode in the NaOH solution is analogous to presynaptic and postsynaptic terminals; the frequency of −5 V acted as a neuronal stimulus. The nonlinearity factor of the potentiation was 0.35 at −5 V as shown in Figure S2. Thus, the voltage condition from −5 to 1 V was applied in the system unless otherwise noted. It was found that synaptic characteristics including nonvolatile behavior, low-power consumption, high-speed operation, programmability, and analog behavior could be optimized depending on the pulse width, duty cycles, and voltage amplitude.

Figure 3 compares the generation of synaptic spike responses at two different pulse widths. It showed that synaptic behavior was observed at a pulse with 0.04 ms in Figure 3a, while the synaptic behavior was not observed at a pulse with 0.08 ms in Figure 3b. It indicated that an optimized pulse condition needs to be developed further. There are several key requirements for synaptic devices including nonvolatile behavior, low-power consumption, high-speed

https://doi.org/10.1021/acsomega.3c05352
ACS Omega 2023, 8, 41495−41501

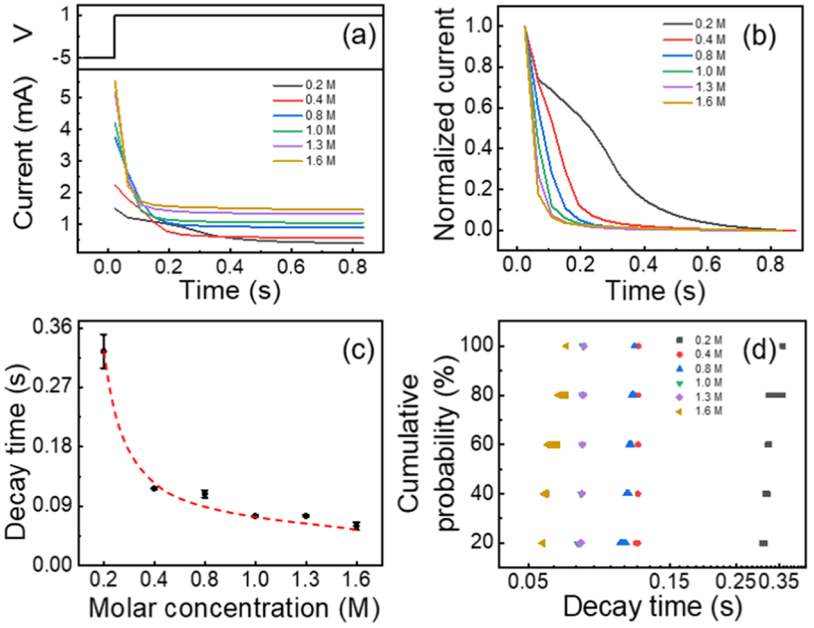

Figure 4. (a) Step response, (b) normalized step response of oxidation current, (c) current decay time, and (d) cumulative probability of Ga electrode in the NaOH solution at different NaOH molar concentrations when the voltage is adjusted from −5 to 1 V.

operation, programmability, and analog behavior. By satisfying these requirements, synaptic devices could serve as an efficient device that can perform complex tasks such as image and speech recognition with high accuracy and speed. Typical learning and forgetting characteristics of the synaptic device are shown in Figure S3.

Figure 4a shows the transient current response generated by the formation of a Ga-based oxide layer on the Ga surface at different NaOH molar concentrations. Once the oxide layer formed on the Ga surface when the voltage changed from −5 to 1 V, a further oxidation reaction was spontaneously prevented. This caused a current reduction over time, and the current finally reached a stable state. The current response showed that both the peak current and the saturation current increased with higher NaOH molar concentrations. The higher peak current was attributed to the higher oxidation reactions, while the higher saturation current was presumably due to the higher ionic conduction in the NaOH solution. As shown in Figure 4b, the current response curve was normalized to compare the current decay behavior at different NaOH molar concentrations.

The current decay time was defined as the time it took for the current to decay from 90 to 10% of its maximum peaks. The results showed that the decay time decreased with higher NaOH molar concentrations, as shown in Figure 4c. The average decay time at 0.2 M was 320 ms, and the value decreased to as low as 60 ms at 1.6 M. Synaptic devices with either long (320 ms) or short (60 ms) decay time can be utilized depending on the specific case and requirement. Synaptic devices with long decay times can be used to store information for extended periods, allowing for the implementation of long-term memory in neuromorphic systems. Synaptic devices with long decay times can also be used for learning and adaptation in response to input patterns. On the other hand, synaptic devices with short decay times can be used to filter out noise and unwanted signals by rapidly reducing the strength of synapses. The synaptic device with different decay times allows for the implementation of a wider range of synaptic plasticity, which can lead to more efficient neuromorphic computing systems. Figure 4d exhibits the cumulative probability of the current decay time at different molar concentrations. Cumulative probability refers to the probability indicating the likelihood of a random variable to assume a value that is equal to or less than a specified value. In other words, it represents the probability of an event occurring up to a certain point in a distribution. This showed that the current decay time in this work could be predicted at certain molar concentrations. The ability to implement different decay times is significant because it can represent a variety of STP/LTP behaviors. This enables the simulation of various synaptic behavior characteristics. This result could be useful for neuromorphic computing applications, which may require specific decay time to function properly.

Figure 5a,b illustrates a schematic drawing of the formation and dissolution reactions of the Ga-based oxide on the Ga electrode at high and low NaOH molar concentrations, showing the different oxidation reactions. The different oxidation mechanisms resulted in various current decay times. It was presumed that a mixed layer of stoichiometric Ga_2O_3 and nonstoichiometric $Ga_2O_{x(x<3)}$ was able to form at lower NaOH molar concentrations. Oxygen atoms in the Ga-oxide layer were supplied from OH^- ions in the NaOH solution. Thus, it was expected that the formation of a nonstoichiometric $Ga_2O_{x(x<3)}$ layer resulted from the low concentration of OH^- ions in the lower NaOH solution at lower NaOH molar concentrations. The nonstoichiometric $Ga_2O_{x(x<3)}$ layer in the mixture would be vulnerable to the NaOH solution and easily dissolve, which would cause new oxidation to occur. This dissolution and partial oxidation would continue at lower NaOH molar concentrations until the surface of the Ga electrode would be entirely covered with the stoichiometric Ga_2O_3 layer, resulting in a slower current decay behavior. In contrast, with higher NaOH molar concentrations, abundant OH^- ions could be supplied near the surface of the Ga electrode when the voltage changed from −5 to 1 V, which could cause the formation of the stoichiometric Ga_2O_3 layer on

https://doi.org/10.1021/acsomega.3c05352
ACS Omega 2023, 8, 41495−41501

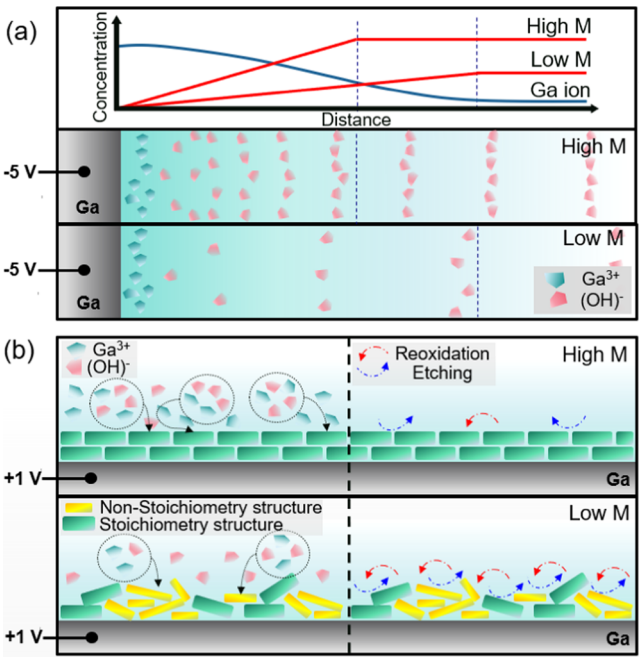

Figure 5. Schematic illustration of the proposed (a) reduction and (b) oxidation mechanisms of the Ga electrode in the NaOH solution at either high or low M.

the Ge electrode. The formed stoichiometric Ga_2O_3 layer might be sufficiently robust in the NaOH solution and thereby prevent further oxidation reactions, which would result in faster current decay behavior. Synaptic properties can be classified into two major categories: short-term plasticity (STP) and long-term plasticity (LTP). STP is a form of synaptic plasticity associated with rapid and transient changes that can last from milliseconds to seconds. STP can filter out noisy and irrelevant information. LTP, on the other hand, is a longer-lasting change in synaptic strength that can last from hours to days or even longer. LTP is thought to relate to many forms of learning and memory. Regarding STP, various types of synaptic devices have been demonstrated to emulate biological synapses. Their typical decay time constants are listed in Figure S1. The results show that the proposed electrochemical oxidation device using liquid Ga in NaOH would be able to cover a wide range of decay times by changing the NaOH molar concentration. Like other liquid-based devices, high-temperature conditions in practical use would be detrimental to the functionality of the device. For example, water in the NaOH solution will start to evaporate at high-temperature conditions. To improve long-term stability such as reliability and endurance characteristics, passivation technology would be further required. The proposed Ga-based device in the NaOH solution was designed to operate under certain temperature conditions that are compatible with the liquid Ga electrode and the NaOH solution. The proposed electrochemical redox device using the liquid Ga electrode in the NaOH solution could replicate the function of biological synapses by utilizing the properties of the liquid Ga electrode and the NaOH solution to produce different decay constants. This could potentially have applications in fields such as artificial intelligence and neural networks, where the ability to replicate the function of biological synapses could be useful. Further research and development to fully understand the potential capabilities and limitations of such a device are necessary.

4. CONCLUSIONS

Synaptic current behavior was demonstrated via a surface electrochemical redox reaction on a liquid Ga electrode in a NaOH solution. By control of the NaOH molar concentration, a wide range of decay time constants were obtained from 60 to 130 ms at 1.6 and 0.2 NaOH molar concentrations, respectively. Synaptic devices with long decay times can be used to store information for extended periods, learning, and adaptation in response to input patterns, while synaptic devices with short decay times can be used to filter out noise and unwanted signals by rapidly reducing the strength of synapses. Our research marks a step forward in the development of flexible and biocompatible neuromorphic devices, which can be utilized for a range of applications where different synaptic strengths are required that can last from a few milliseconds to seconds.

■ ASSOCIATED CONTENT

Supporting Information

The Supporting Information is available free of charge at https://pubs.acs.org/doi/10.1021/acsomega.3c05352.

Benchmark for the synaptic current decay time with various synaptic devices, nonlinearity analysis of the potentiation at −2 and −5 V, and learning and forgetting characteristics of the synaptic device (PDF)

■ AUTHOR INFORMATION

Corresponding Author

Wan Sik Hwang − *Department of Materials Science and Engineering, Korea Aerospace University, Goyang 10540, Republic of Korea; Department of Smart Air Mobility, Korea Aerospace University, Goyang 10540, Republic of Korea;* orcid.org/0000-0002-0060-9348; Email: whwang@kau.ac.kr

Authors

Dahee Seo − *Department of Materials Science and Engineering, Korea Aerospace University, Goyang 10540, Republic of Korea; Department of Smart Air Mobility, Korea Aerospace University, Goyang 10540, Republic of Korea*

Seongyeon Kang − *Department of Materials Science and Engineering, Korea Aerospace University, Goyang 10540, Republic of Korea*

Heejoong Ryou − *Department of Materials Science and Engineering, Korea Aerospace University, Goyang 10540, Republic of Korea; Department of Smart Air Mobility, Korea Aerospace University, Goyang 10540, Republic of Korea*

Myunghun Shin − *School of Electronics and Information Engineering, Korea Aerospace University, Goyang 10540, Republic of Korea*

Complete contact information is available at: https://pubs.acs.org/10.1021/acsomega.3c05352

Author Contributions

‖D.S. and S.K. contributed equally to this work.

Notes

The authors declare no competing financial interest.

https://doi.org/10.1021/acsomega.3c05352
ACS Omega 2023, 8, 41495−41501

■ ACKNOWLEDGMENTS

This work was financially supported by the Ministry of Small and Medium-sized Enterprises (SMEs) and Startups (MSS), Korea, under the "Regional Specialized Industry Development Plus Program(R&D, S3365219)" supervised by the Korea Technology and Information Promotion Agency (TIPA).

■ REFERENCES

(1) Arikpo, I. I.; Ogban, F. U.; Eteng, I. E. Von Neumann architecture and modern computers. *Global J. Math. Sci.* **2007**, *6*, 97−103.
(2) Zidan, M. A.; Strachan, J. P.; Lu, W. D. The future of electronics based on memristive systems. *Nat. Electron.* **2018**, *1*, 22−29.
(3) Smith, S. L.; Häusser, M. Parallel processing of visual space by neighboring neurons in mouse visual cortex. *Nat. Neurosci.* **2010**, *13*, 1144−1149.
(4) Petrenko, S. *Big Data Technologies for Monitoring of Computer Security: A Case Study of the Russian Federation*; Springer, 2018; pp 1−249.
(5) Ahn, J.; Hong, S.; Yoo, S.; Mutlu, O.; Choi, K. In *A Scalable Processing-in-Memory Accelerator for Parallel Graph Processing*, Proceedings of the 42nd Annual International Symposium on Computer Architecture, 2015; pp 105−117.
(6) Chi, P.; Li, S.; Xu, C.; Zhang, T.; Zhao, J.; Liu, Y.; Wang, Y.; Xie, Y. Prime: A novel processing-in-memory architecture for neural network computation in reram-based main memory. *ACM SIGARCH Comput. Architect. News* **2016**, *44*, 27−39.
(7) Wang, C.; He, W.; Tong, Y.; Zhang, Y.; Huang, K.; Song, L.; Zhong, S.; Ganeshkumar, R.; Zhao, R. Memristive devices with highly repeatable analog states boosted by graphene quantum dots. *Small* **2017**, *13*, No. 1603435.
(8) Zhu, X.; Lee, S. H.; Lu, W. D. Nanoionic Resistive-Switching Devices. *Adv. Electron. Mater.* **2019**, *5*, No. 1900184.
(9) Huang, W.; Xia, X.; Zhu, C.; Steichen, P.; Quan, W.; Mao, W.; Yang, J.; Chu, L.; Li, X. Memristive artificial synapses for neuromorphic computing. *Nano-Micro Lett.* **2021**, *13*, No. 85.
(10) Siddik, A.; Haldar, P. K.; Paul, T.; Das, U.; Barman, A.; Roy, A.; Sarkar, P. K. Nonvolatile resistive switching and synaptic characteristics of lead-free all-inorganic perovskite-based flexible memristive devices for neuromorphic systems. *Nanoscale* **2021**, *13*, 8864−8874.
(11) Shen, Z.; Zhao, C.; Qi, Y.; Xu, W.; Liu, Y.; Mitrovic, I. Z.; Yang, L.; Zhao, C. Advances of RRAM devices: Resistive switching mechanisms, materials and bionic synaptic application. *Nanomaterials* **2020**, *10*, No. 1437.
(12) Faria, G. C.; Duong, D. T.; Salleo, A. On the transient response of organic electrochemical transistors. *Org. Electron.* **2017**, *45*, 215−221.
(13) He, Z.; Gou, F.; Chen, R.; Yin, K.; Zhan, T.; Wu, S. Liquid crystal beam steering devices: principles, recent advances, and future developments. *Crystals* **2019**, *9*, No. 292.
(14) Wan, Q.; Zeng, F.; Yin, J.; Sun, Y.; Hu, Y.; Liu, J.; Wang, Y.; Li, G.; Guo, D.; Pan, F. Phase-change nanoclusters embedded in a memristor for simulating synaptic learning. *Nanoscale* **2019**, *11*, 5684−5692.
(15) Sarwat, S. G.; Kersting, B.; Moraitis, T.; Jonnalagadda, V. P.; Sebastian, A. Phase-change memtransistive synapses for mixed-plasticity neural computations. *Nat. Nanotechnol.* **2022**, *17*, 507−513.
(16) Kim, S.; Heo, K.; Lee, S.; Seo, S.; Kim, H.; Cho, J.; Lee, H.; Lee, K.; Park, J. Ferroelectric polymer-based artificial synapse for neuromorphic computing. *Nanoscale Horiz.* **2021**, *6*, 139−147.
(17) Kwon, K. C.; Zhang, Y.; Wang, L.; Yu, W.; Wang, X.; Park, I.; Choi, H. S.; Ma, T.; Zhu, Z.; Tian, B.; et al. In-plane ferroelectric tin monosulfide and its application in a ferroelectric analog synaptic device. *ACS Nano* **2020**, *14*, 7628−7638.
(18) Ham, S.; Kang, M.; Jang, S.; Jang, J.; Choi, S.; Kim, T.; Wang, G. One-dimensional organic artificial multi-synapses enabling electronic textile neural network for wearable neuromorphic applications. *Sci. Adv.* **2020**, *6*, No. eaba1178.
(19) Luo, Z.-D.; Xia, X.; Yang, M.; Wilson, N. R.; Gruverman, A.; Alexe, M. Artificial optoelectronic synapses based on ferroelectric field-effect enabled 2D transition metal dichalcogenide memristive transistors. *ACS Nano* **2020**, *14*, 746−754.
(20) Van De Burgt, Y.; Lubberman, E.; Fuller, E. J.; Keene, S. T.; Faria, G. C.; Agarwal, S.; Marinella, M. J.; Talin, A. A.; Salleo, A. A non-volatile organic electrochemical device as a low-voltage artificial synapse for neuromorphic computing. *Nat. Mater.* **2017**, *16*, 414−418.
(21) Zhu, L. Q.; Wan, C. J.; Guo, L. Q.; Shi, Y.; Wan, Q. Artificial synapse network on inorganic proton conductor for neuromorphic systems. *Nat. Commun.* **2014**, *5*, No. 3158.
(22) Xu, W.; Cho, H.; Kim, Y.; Kim, Y.; Wolf, C.; Park, C.; Lee, T. Organometal halide perovskite artificial synapses. *Adv. Mater.* **2016**, *28*, 5916−5922.
(23) Park, H.; Kim, H.; Lim, D.; Zhou, H.; Kim, Y.; Lee, Y.; Park, S.; Lee, T. Retina-inspired carbon nitride-based photonic synapses for selective detection of UV light. *Adv. Mater.* **2020**, *32*, No. 1906899.
(24) Lee, Y.; Lee, T. Organic synapses for neuromorphic electronics: from brain-inspired computing to sensorimotor nervetronics. *Acc. Chem. Res.* **2019**, *52*, 964−974.
(25) Go, G.-T.; Lee, Y.; Seo, D.; Pei, M.; Lee, W.; Yang, H.; Lee, T. Achieving microstructure-controlled synaptic plasticity and long-term retention in ion-gel-gated organic synaptic transistors. *Adv. Intell. Syst.* **2020**, *2*, No. 2000012.
(26) He, Y.; Liu, R.; Jiang, S.; Chen, C.; Zhu, L.; Shi, Y.; Wan, Q. IGZO-based floating-gate synaptic transistors for neuromorphic computing. *J. Phys. D: Appl. Phys.* **2020**, *53*, No. 215106.
(27) Zhang, M.; Fan, Z.; Jiang, X.; Zhu, H.; Chen, L.; Xia, Y.; Yin, J.; Liu, X.; Sun, Q.; Zhang, D. W. MoS2-based charge-trapping synaptic device with electrical and optical modulated conductance. *Nanophotonics* **2020**, *9*, 2475−2486.
(28) Ji, X.; Paulsen, B. D.; Chik, G. K.; Wu, R.; Yin, Y.; Chan, P. K.; Rivnay, J. Mimicking associative learning using an ion-trapping non-volatile synaptic organic electrochemical transistor. *Nat. Commun.* **2021**, *12*, No. 2480.
(29) Seo, D.; Ryou, H.; Hong, S. W.; Seo, J. H.; Shin, M.; Hwang, W. S. Synaptic Current Response of a Liquid Ga Electrode via a Surface Electrochemical Redox Reaction in a NaOH Solution. *ACS Omega* **2022**, *7*, 19872−19878.
(30) Kim, D.; Lee, J.-S. Liquid-based memory devices for next-generation computing. *ACS Appl. Electron. Mater.* **2023**, *5*, 664−673.
(31) Melianas, A.; Quill, T. J.; LeCroy, G.; Tuchman, Y.; Loo, Hv.; Keene, S. T.; Giovannitti, A.; Lee, H. R.; Maria, I. P.; McCulloch, I.; Salleo, A. Temperature-resilient solid-state organic artificial synapses for neuromorphic computing. *Sci. Adv.* **2020**, *6*, No. eabb2958.
(32) Zhao, S.; Ni, Z.; Tan, H.; Wang, Y.; Jin, H.; Nie, T.; Xu, M.; Pi, X.; Yang, D. Electroluminescent synaptic devices with logic functions. *Nano Energy* **2018**, *54*, 383−389.
(33) Bian, H.; Goh, Y. Y.; Liu, Y.; Ling, H.; Xie, L.; Liu, X. Stimuli-Responsive Memristive Materials for Artificial Synapses and Neuromorphic Computing. *Adv. Mater.* **2021**, *33*, No. 2006469.
(34) Xu, M.; Mai, X.; Lin, J.; Zhang, W.; Li, Y.; He, Y.; Tong, H.; Hou, X.; Zhou, P.; Miao, X. Recent advances on neuromorphic devices based on chalcogenide phase-change materials. *Adv. Funct. Mater.* **2020**, *30*, No. 2003419.
(35) Wang, Y.; Yin, L.; Huang, W.; Li, Y.; Huang, S.; Zhu, Y.; Yang, D.; Pi, X. Optoelectronic synaptic devices for neuromorphic computing. *Adv. Intell. Syst.* **2021**, *3*, No. 2000099.
(36) Battistoni, S.; Cocuzza, M.; Marasso, S. L.; Verna, A.; Erokhin, V. The role of the internal capacitance in organic memristive device for neuromorphic and sensing applications. *Adv. Electron. Mater.* **2021**, *7*, No. 2100494.
(37) Kanehira, S.; Kanamori, S.; Nagashima, K.; Saeki, T.; Visbal, H.; Fukui, T.; Hirao, K. Controllable hydrogen release via aluminum powder corrosion in calcium hydroxide solutions. *J. Asian Ceram. Soc.* **2013**, *1*, 296−303.

https://doi.org/10.1021/acsomega.3c05352
ACS Omega 2023, 8, 41495−41501

(38) Gough, R. C.; Dang, J. H.; Moorefield, M. R.; Zhang, G. B.; Hihara, L. H.; Shiroma, W. A.; Ohta, A. T. Self-actuation of liquid metal via redox reaction. *ACS Appl. Mater. Interfaces* **2016**, *8*, 6−10.
(39) Kunze, J.; Maurice, V.; Klein, L. H.; Strehblow, H.-H.; Marcus, P. In situ STM study of the duplex passive films formed on Cu(111) and Cu(001) in 0.1 M NaOH. *Corros. Sci.* **2004**, *46*, 245−264.

https://doi.org/10.1021/acsomega.3c05352
ACS Omega 2023, 8, 41495−41501